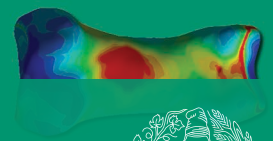
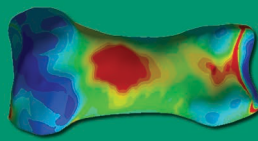
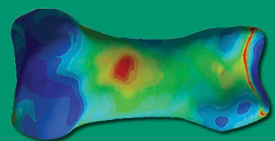
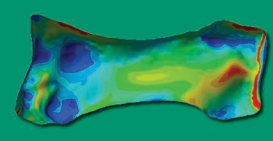
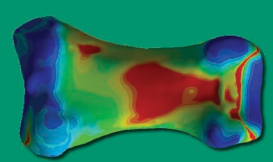
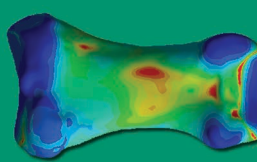
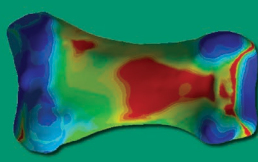
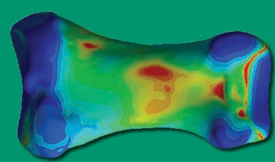
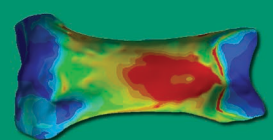
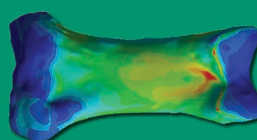
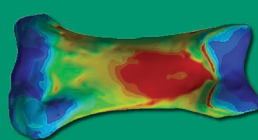
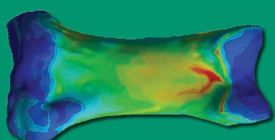
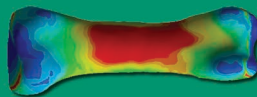


Finite element analysis of the proximal phalanx of the thumb in Hominoidea during simulated stone tool use



Ana BUCCHI, Thomas A. PÜSCHEL,
Carlos LORENZO & Jordi MARCÉ-NOGUÉ



DIRECTEURS DE LA PUBLICATION / *PUBLICATION DIRECTORS*:

Bruno David, Président du Muséum national d'Histoire naturelle
Étienne Ghys, Secrétaire perpétuel de l'Académie des sciences

RÉDACTEURS EN CHEF / *EDITORS-IN-CHIEF*: Michel Laurin (CNRS), Philippe Taquet (Académie des sciences)

ASSISTANTE DE RÉDACTION / *ASSISTANT EDITOR*: Adenise Lopes (Académie des sciences; cr-palevol@academie-sciences.fr)

MISE EN PAGE / *PAGE LAYOUT*: Martin Wable (Muséum national d'Histoire naturelle; martin.wable@mnhn.fr)

RÉDACTEURS ASSOCIÉS / *ASSOCIATE EDITORS*:

Micropaléontologie/*Micropalaeontology*

Maria Rose Petrizzi (Università di Milano, Milano)

Paléobotanique/*Palaeobotany*

Cyrille Prestianni (Royal Belgian Institute of Natural Sciences, Brussels)

Métazoaires/*Metazoa*

Annalisa Ferretti (Università di Modena e Reggio Emilia, Modena)

Paléoichthyologie/*Palaeoichthyology*

Philippe Janvier (Muséum national d'Histoire naturelle, Académie des sciences, Paris)

Amniotes du Mésozoïque/*Mesozoic amniotes*

Hans-Dieter Sues (Smithsonian National Museum of Natural History, Washington)

Tortues/*Turtles*

Juliana Sterli (CONICET, Museo Paleontológico Egidio Feruglio, Trelew)

Lépidosauromorphes/*Lepidosauromorphs*

Hussam Zaher (Universidade de São Paulo)

Oiseaux/*Birds*

Eric Buffetaut (CNRS, École Normale Supérieure, Paris)

Paléomammalogie (petits mammifères)/*Palaeomammalogy* (small mammals)

Robert Asher (Cambridge University, Cambridge)

Paléomammalogie (mammifères de moyenne et grande taille)/*Palaeomammalogy* (large and mid-sized mammals)

Lorenzo Rook (Università degli Studi di Firenze, Firenze)

Paléoanthropologie/*Palaeoanthropology*

Roberto Macchiarelli (Université de Poitiers, Poitiers)

Archéologie préhistorique/*Prehistoric archaeology*

Marcel Otte (Université de Liège, Liège)

COUVERTURE / *COVER*:

Composition à partir d'illustrations de l'article / Made from the Figures of the article.

Comptes Rendus Palevol est indexé dans / *Comptes Rendus Palevol* is indexed by:

- Cambridge Scientific Abstracts
- Current Contents® Physical
- Chemical, and Earth Sciences®
- ISI Alerting Services®
- Geoabstracts, Geobase, Georef, Inspec, Pascal
- Science Citation Index®, Science Citation Index Expanded®
- Scopus®

Les articles ainsi que les nouveautés nomenclaturales publiés dans *Comptes Rendus Palevol* sont référencés par :

Articles and nomenclatural novelties published in Comptes Rendus Palevol are registered on:

- ZooBank® (<http://zoobank.org>)

Comptes Rendus Palevol est une revue en flux continu publiée par les Publications scientifiques du Muséum, Paris et l'Académie des sciences, Paris
Comptes Rendus Palevol is a fast track journal published by the Museum Science Press, Paris and the Académie des sciences, Paris

Les Publications scientifiques du Muséum publient aussi / *The Museum Science Press also publish:*

Adansonia, Geodiversitas, Zoosystema, Anthropozoologica, European Journal of Taxonomy, Naturae, Cryptogamie sous-sections *Algologie, Bryologie, Mycologie*.

L'Académie des sciences publie aussi / *The Académie des sciences also publishes:*

Comptes Rendus Mathématique, Comptes Rendus Physique, Comptes Rendus Mécanique, Comptes Rendus Chimie, Comptes Rendus Géoscience, Comptes Rendus Biologies.

Diffusion – Publications scientifiques Muséum national d'Histoire naturelle

CP 41 – 57 rue Cuvier F-75231 Paris cedex 05 (France)

Tél.: 33 (0)1 40 79 48 05 / Fax: 33 (0)1 40 79 38 40

diff.pub@mnhn.fr / <http://sciencepress.mnhn.fr>

Académie des sciences, Institut de France, 23 quai de Conti, 75006 Paris.

© Publications scientifiques du Muséum national d'Histoire naturelle / © Académie des sciences, Paris, 2020

ISSN (imprimé / print): 1631-0683/ ISSN (électronique / electronic): 1777-571X

Finite element analysis of the proximal phalanx of the thumb in Hominoidea during simulated stone tool use

BUCCHI Ana

Institut Català de Paleoecologia Humana i Evolució Social (IPHES)
and Area de Prehistòria, Universitat Rovira i Virgili (URV), Tarragona (Spain)
anabucchi@gmail.com (corresponding author)

PÜSCHEL Thomas A.

Primate Models for Behavioural Evolution Lab, Institute of Cognitive and Evolutionary
and Anthropology, University of Oxford, Oxford (United Kingdom)

LORENZO Carlos

Institut Català de Paleoecologia Humana i Evolució Social (IPHES)
and Area de Prehistòria, Universitat Rovira i Virgili (URV), Tarragona (Spain)

MARCÉ-NOGUÉ Jordi

Center of Natural History, University of Hamburg, Hamburg (Germany)
and Institut Català de Paleontologia M. Crusafont,
Universitat Autònoma de Barcelona, Barcelona (Spain)

Submitted on 17 August 2019 | accepted on 18 October 2019 | published on 10 August 2020

[urn:lsid:zoobank.org:pub:F8B46233-7A54-4C19-8183-3B533AFA4DC8](https://doi.org/10.5852/palevol2020v19a2)

Bucchi A., Püschel T. A., Lorenzo C. & Marcé-Nogué J. 2020. — Finite element analysis of the proximal phalanx of the thumb in Hominoidea during simulated stone tool use. *Comptes Rendus Palevol* 19 (2): 26-39. <https://doi.org/10.5852/palevol2020v19a2>

ABSTRACT

Finite element analysis was applied to analyze six individuals from different primate species (*Homo sapiens* Linnaeus, 1758, *Homo neanderthalensis* King, 1864, *Pan troglodytes* Blumenbach, 1779, *Gorilla gorilla* Savage, 1847, *Pongo pygmaeus* Linnaeus, 1760 and *Hylobates lar* Linnaeus, 1771) to identify stress distribution patterns on the pollical proximal phalanx during simulated hammerstone use. We expected the stress to be better distributed in our species than in other hominids based on the idea that, unlike apes, the human hand is adapted to tool-related behaviors. Our results indicate that the human phalanx unevenly distributes stresses and is one of the most fragile of all, especially when a small hammerstone is simulated. Tool orientation relative to the phalanx did not have a substantial effect on average stress or distribution. We conclude that great apes can resist loads exerted during this activity more efficiently than humans and that there were probably other evolutionary factors acting on this bone in our species.

KEY WORDS

Functional morphology,
hand evolution,
primates,
stress.

RÉSUMÉ

Analyse par éléments finis de la phalange proximale du pouce des Hominoidea pendant l'utilisation simulée d'outils lithiques.

Une analyse par méthode des éléments finis a été appliquée à six individus représentant différentes espèces de primates (*Homo sapiens* Linnaeus, 1758, *Homo neanderthalensis* King, 1864, *Pan troglodytes* Blumenbach, 1779, *Gorilla gorilla* Savage, 1847, *Pongo pygmaeus* Linnaeus, 1760 et *Hylobates lar* Linnaeus, 1771) pour identifier les patrons de distribution des contraintes au niveau de la phalange proximale du pouce, pendant l'utilisation d'un percuteur. Nous avons émis l'hypothèse que les contraintes étaient mieux distribuées dans notre espèce que chez les autres hominidés en se basant sur le postulat que, à l'inverse des grands singes, la main humaine est adaptée aux comportements liés à l'utilisation d'outils. Nos résultats indiquent que la phalange humaine distribue les contraintes de manière inégale et est une des plus fragiles de tout l'échantillonnage testé, notamment quand l'utilisation d'un petit percuteur est simulée. L'orientation de l'outil par rapport à la phalange n'a pas montré d'effet substantiel sur les contraintes moyennes ou leur distribution. Nous concluons que les grands singes peuvent mieux résister que les humains à des contraintes subies durant cette activité et qu'il y a probablement d'autres facteurs évolutifs agissant sur la structure osseuse de notre espèce.

MOTS CLÉS
Morphologie fonctionnelle,
évolution de la main,
primates,
stress.

INTRODUCTION

There is a widespread idea that the derived manual anatomy of humans is a result of selective pressures related to manipulative behaviors (e.g. Hamrick *et al.* 1998; Young 2003; Key & Dunmore 2015; Skinner *et al.* 2015; Kivell *et al.* 2016) as, among primates, humans exert unique, more efficient precision and power grips (e.g. Niewoehner 2001; Shrewsbury *et al.* 2003; Tocheri *et al.* 2003; Rolian *et al.* 2011; Marzke 2013; Key & Dunmore 2015; Bardo *et al.* 2017). Unlike humans, locomotion constitutes the primarily selective pressure on the hand for most primates (e.g. Tuttle 1969; Jouffroy *et al.* 1991). This is not to say that non-humans primates are unable of performing tool-based activities, as they have been reported in other primates (Pruett & Bertolani 2007; Wynn *et al.* 2011; Gumert & Malaivijitnond 2013; Visalberghi *et al.* 2015), and some of their tools, including stone hammers, and the behaviors involved (e.g. direct hard hammer knapping) are very similar or indistinguishable from Oldowan culture (Wynn & McGrew 1989; Wynn *et al.* 2011). However, the manual pressures and high muscle activities experienced by the hand during travel (Susman & Stern 1979; Wunderlich & Jungers 2009; Matarazzo 2013; Samuel *et al.* 2018) play a more important role.

The selective pressures related to stone tool use supposedly started early in the human lineage. The intrinsic muscles of the thumb show high level forces during hard hammer percussion manufacture of Oldowan tools (Hamrick *et al.* 1998; Marzke *et al.* 1998). The thumb also experiences significant pressures during stone tool production (Key & Dunmore 2015; Williams-Hatala *et al.* 2018). In addition, some derived morphology facilitating manipulation of stone tools, as the expanded apical tuft of the distal thumb phalanx, were already present in *Orrorin* (Gommery & Senut 2006), although numerous derived conditions evolved later in a mosaic fashion until the fully-derived hand of Neanderthals and modern humans (for a review, see Tocheri *et al.* 2008, and also Key & Dunmore 2018). Changes in hominins in the shortening of the fingers relative to thumb length, which ensures the human-like precision grip capability, occurred in *Australopithecus* (Alba *et al.* 2003; Green & Gordon

2008; Tocheri *et al.* 2008). Robust first metacarpals have been identified in early *Homo/Paranthropus* (Susman 1988), which helps to produce stronger, efficient grips and tolerate higher joint stresses (Rolian *et al.* 2011; Key & Dunmore 2015; Key & Lycett 2018).

Even though most of the paleoanthropological literature agrees that hands of humans and non-human primates are adapted to different functions (i.e., manipulation vs locomotion), recent studies have concluded that some derived traits leading towards *Homo* (e.g. finger proportions) are not the product of selective pressures acting directly on the hands but on other region of the skeleton (i.e., the foot) (Rolian *et al.* 2010) which are related to terrestriality (Heldstab *et al.* 2016; Bardo *et al.* 2017) and were subsequently exapted for tool manipulation. This can explain why skillful hands were present long before the first record of lithic industry (Alba *et al.* 2003; Almécija *et al.* 2010). How humans acquired this unique configuration of musculoskeletal traits in the hand which facilitates tool related behaviors has profound implications in our understanding of human evolution overall, considering that stone technology is a key element defining culture in our species (e.g. Foley & Lahr 2003). However, testing biological causality is hard to address and we may never be absolutely certain on the evolutionary mechanisms having shaped the human hand. Consequently, we think that new insights are needed to better assess whether the evolution of the human hand is driven by tool-related behaviors.

Here we use finite element analysis (FEA) to evaluate if stress on the human pollical proximal phalanx (PP1) fits with the functional adaptation (to tool use) hypothesis for the evolution of our hand. This method makes it possible to control and repeat biomechanical scenarios under modifiable conditions (for a review, see Rayfield 2007) making it suitable for morpho-functional problems such as this. To our knowledge, no study has applied FEA to evaluate the effect of stone tool use on the hand.

The stress distribution in the PP1 was analyzed in six Hominoidea taxa (*Homo sapiens* Linnaeus, 1758, *Homo neanderthalensis* King, 1864, *Pan troglodytes* Blumenbach, 1779, *Gorilla gorilla* Savage, 1847, *Pongo pygmaeus* Linnaeus, 1760 and *Hylobates lar*

TABLE 1. — Sample. Abbreviations: **a**, age of individuals, if known; unk: unknown. **b**, M: male; F: female. **c**, R: right; L: left.

Species	Common name	Age ^a	Sex ^b	Side	Digital database/ n°	CT/microCT resolution (mm)
<i>Homo sapiens</i>	Modern human	59	M	R	None	0.08
<i>Homo neanderthalensis</i>	Neanderthal	unk	unk	R	NESPOS/ Krapina 202	0.03
<i>Pan troglodytes</i>	Chimpanzee	29	M	L	KUPRI/345	0.219
<i>Gorilla gorilla</i>	Gorilla	38	M	R	KUPRI/1353	0.500
<i>Pongo pygmaeus</i>	Orangutan	32	F	R	None	0.03
<i>Hylobates lar</i>	Gibbon	33	M	R	KUPRI/465	0.250

TABLE 2. — Percentage of main locomotor behavoir of the non-human sample, according to Hunt (2004).

Taxon	Climb	Braquiate	Clamber	Walk
Chimpanzee	6.5	0.8	0.0	89.9
Gorilla	19.7	3.6	0.0	64.4
Orangutan	31.3	15.5	40.7	12.0
Gibbon	34.2	51.2	0.0	0.0

Linnaeus, 1771) (Table 1) under loading conditions related to hard hammer percussion to describe stress patterns on PP1s during the same task. We expect to find that the human PP1s distribute stresses differently than apes, as hands in humans and apes show morphologically commitment to different functions – manipulation and locomotion (Table 2) – and the loading condition simulated here are related to stone tool use. In particular, we expect that the human phalanges distribute stresses more efficiently and can withstand the stresses related to hammerstone use better than our closest living relatives.

MATERIAL AND METHODS

SAMPLE AND DIGITALIZATION

A recent modern human, a Neanderthal from Krapina (Vi 202) and four extant non-human hominoids were analyzed: chimpanzee, gorilla, orangutan and gibbon. All specimens were adults with no evident pathologies (Table 1).

The PP1 from the human individual was obtained from a fresh cadaver and scanned with a micro-CT (Perkin Elmer, model Quantum Fx, Hopkinton MA, United States). The orangutan PP1 is from the Senckenberg Museum in Frankfurt, Germany (SMF 74303) and was scanned on a BIR ACTIS 225/330 micro-CT scanner at the Department of Human Evolution, Max Planck Institute for Evolutionary Anthropology (Leipzig, Germany). The remaining specimens were obtained from digital databases; the micro-CT of the Neanderthal PP1 from NESPOS (www.nespos.org/display/PublicNesposSpace/Human+Fossils), whereas the CT scans from the rest of the non-human sample were downloaded from the Digital Morphology Museum, Kyoto University, Japan (KUPRI; dmm.pri.kyoto-u.ac.jp/dmm/WebGallery/index.html). Even though KUPRI CT scans have a relative low resolution (Table 1) and do not allow to observe bone segments in high detail, they can still provide relevant morphological information, as it has been shown that even medium-resolution scans can accurately quantify shape (Slizewski *et al.* 2010;

McCurry *et al.* 2015). In fact, it has been shown that this resolution is sufficiently accurate to even identify intra-specific differences of relatively small specimens (Marcy *et al.* 2018).

In order to make models from different resolution scans comparable, trabecular bone was enclosed using the “Convex Hull” tool in Meshlab v.2016.12 (Cignoni *et al.* 2008) and the same mechanical properties were defined for all the specimens. Elements were then converted to CAD models. During this last step, irregularities in the surface caused by segmentation were repaired using refinement and smoothing tools (Lautenschlager 2016) in Geomagic Studio® (3D Systems, v. 12, Rock Hill, SC, United States).

All scans were segmented using Seg3D software (CIBC, v. 2.4.0, 2017). The medullary cavity, trabeculae and compact bone were segmented on the specimens by applying a combination of case-specific thresholding values and manual painting techniques. Models of left PP1's (Table 1) were reflected to enable meaningful comparisons.

To avoid possible problems when aligning different individuals (due to inter-specific morphological differences), we selected one individual as a reference (i.e., the chimpanzee representative) to perform a best-fit alignment to align all the models according to a common reference plane. This procedure was carried out in Geomagic Studio® (3D Systems, v. 12, Rock Hill, SC, United States) prior to FEA to align all the models, so that loads could be applied in the same axis and allow an easier interpretation of the results.

MODEL PROPERTIES

Structural static analysis was performed to evaluate the biomechanical behavior of the PP1s using the Finite Element Package ANSYS 17.1 in a Dell Precision™ Workstation T5500 with 48 GB and 5.33 GHz. Elastic, linear and homogeneous material properties were assumed for the cortical bone using the values of E (Young's modulus) 18.6 GPa and v (Poisson's ratio) 0.3, while for trabecular bone values of E 0.75 GPa and v 0.3 were assumed (Butz *et al.* 2012).

In this study, the focus in the comparison of the models is primarily on the von Mises stress distribution. Bone can be modeled as a brittle (Doblaré *et al.* 2004) or ductile (Dumont *et al.* 2009) material. According to Doblaré *et al.* (2004), the von Mises criterion is the most commonly applied and useful criterion for predicting the yield and fracture location in bone when ductile and isotropic material properties are assumed in cortical bone. The PP1 models were meshed using an adaptive hexahedral mesh and ANSYS® (Marcé-Nogué

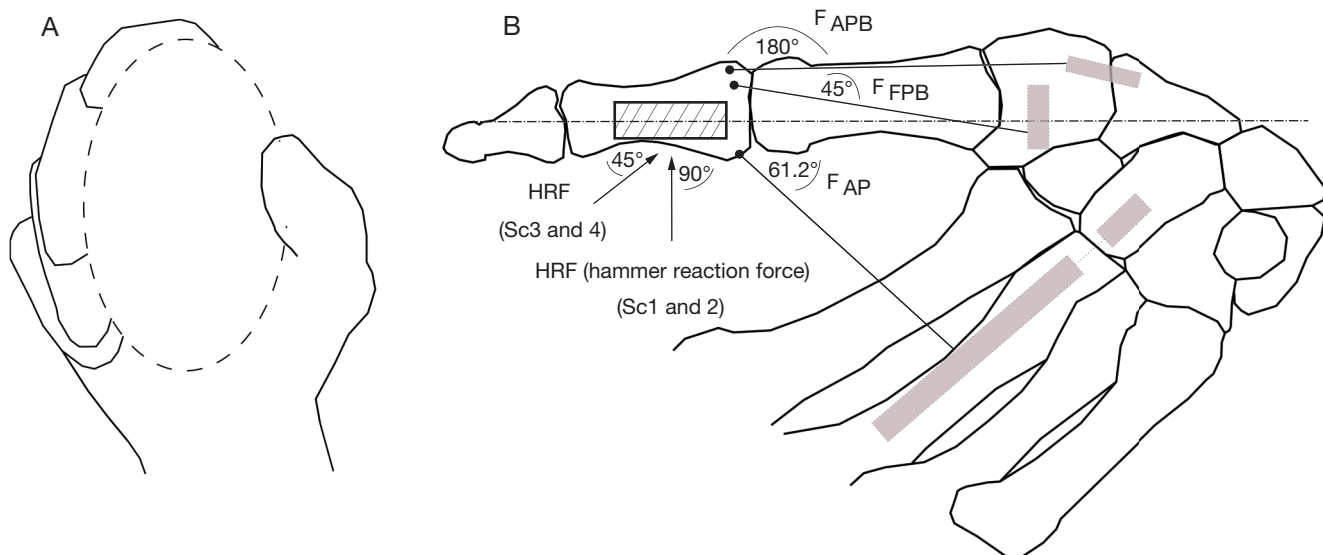


FIG. 1. — Biomechanical model of hammerstone use: **B**, corresponds to a zoom in palmar view of the area of interest during **A**, the grip of a human individual (based on Marzke *et al.* 1998). **B**, shows the angles of the muscular forces acting on the PP1. HRF is in 90° relative to the horizontal line for scenarios 1 and 2 and in 45° for scenarios 2 and 4. This force was applied on the entire palmar surface of the PP1 except in the joint areas and is represented with a hatched rectangle. Angles of the muscle forces are shown relative to the horizontal line. Abbreviations: **FAP**, Adductor Pollicis Force; **FAPB**, Abductor Pollicis Brevis Force; **FFPB**, Flexor Pollicis Brevis Force; **EPB**, direction force was applied in 16.7° and is not showed here as it attached on the dorsal surface of the PP1. Grey rectangles represent the origin areas of the muscles.

TABLE 3. — Mesh characteristics for each one of the specimens. Abbreviations: **a**, volume of the cortical bone; **b**, volume of trabecular bone; **c**, number of elements used to create the mesh for each FE model.

Specimen	Volume CB (mm ³) ^a	Volume TB (mm ³) ^b	N elements ^c
Modern human	1012.8	651.1	225729
Neanderthal	733.3	662.6	240469
Chimpanzee	1046.1	178.6	160103
Gorilla	1642.9	577.9	225710
Orangutan	610.1	542.8	199857
Gibbon	250.7	65.9	311431

et al. 2015). The model meshes ranged between 200.000 and 320.000 elements depending on the particular specimen and loading scenario (Table 3).

LOADING SCENARIOS AND BOUNDARY CONDITIONS

The hands were modeled using a free-body diagram approach in a precision three-jaw chuck grip (Fig. 1), following Marzke *et al.* (1998), since we obtained the applied muscle recruitment data from their study.

Forty-eight loading cases were generated. These included two hammerstone orientations relative to the PP1 and two muscle activity patterns associated with differences in hammerstone mass for the six individuals under study (Figs 1; 2). We also generated two different scaling scenarios for muscular data considering that for only two species (*Homo sapiens* and *Pan troglodytes*) there is enough muscular information to perform the simulations.

In the first scaling scenario, we scaled the forces of the Neanderthal, chimpanzee, gorilla, orangutan and gibbon using

the extant human data as a reference, whereas in the second one, we used the chimpanzee muscular data as a reference to scale the forces of all the other representatives. In each of these two settings, the loads of the remaining specimens were scaled relative to the individuals of reference to yield identical force, i.e., the volume ratios (supplementary data Appendix 1). This way differences in stress distribution can be interpreted entirely as result of shape differences (Dumont *et al.* 2009). These values of muscular contraction pressure were calculated according to the method developed by Marcé-Nogué *et al.* (2013) and rearranged for 3D models by Fortuny *et al.* (2015).

Equation for this is $F_A = \left(\frac{V_A}{V_B} \right)^{\frac{2}{3}} F_B$, where F_A is the scaled force, F_B the reference force, and V_A and V_B the respective volumes for CB.

For the human, muscle forces were calculated by means of the physiological cross-sectional area (PCSA) collected from the forearm of a fresh cadaver of a 59-year-old man. All muscles attached at the PP1 were dissected: abductor pollicis brevis (APB), extensor pollicis brevis (EPB), flexor pollicis brevis (FPB), and adductor pollicis (AP) (cf. Sacks & Roy 1982). The PCSA obtained from the human cadaver were the following: FPB (0.6612 cm²), ADP (1.429 cm²), EPB (0.2121 cm²), and APB (0.2587 cm²). The insertion areas of the muscles involved were defined in the model to apply the forces of muscular contraction. The angles of the muscle tendons were estimated *in situ*. For the remaining specimens, tendon angles were assumed to be the same as for the human (Appendix 1), as areas of the bone in which muscles attached are similar between them (Diogo *et al.* 2011, 2012a, 2013a, b). PCSAs for chimpanzees were obtained from

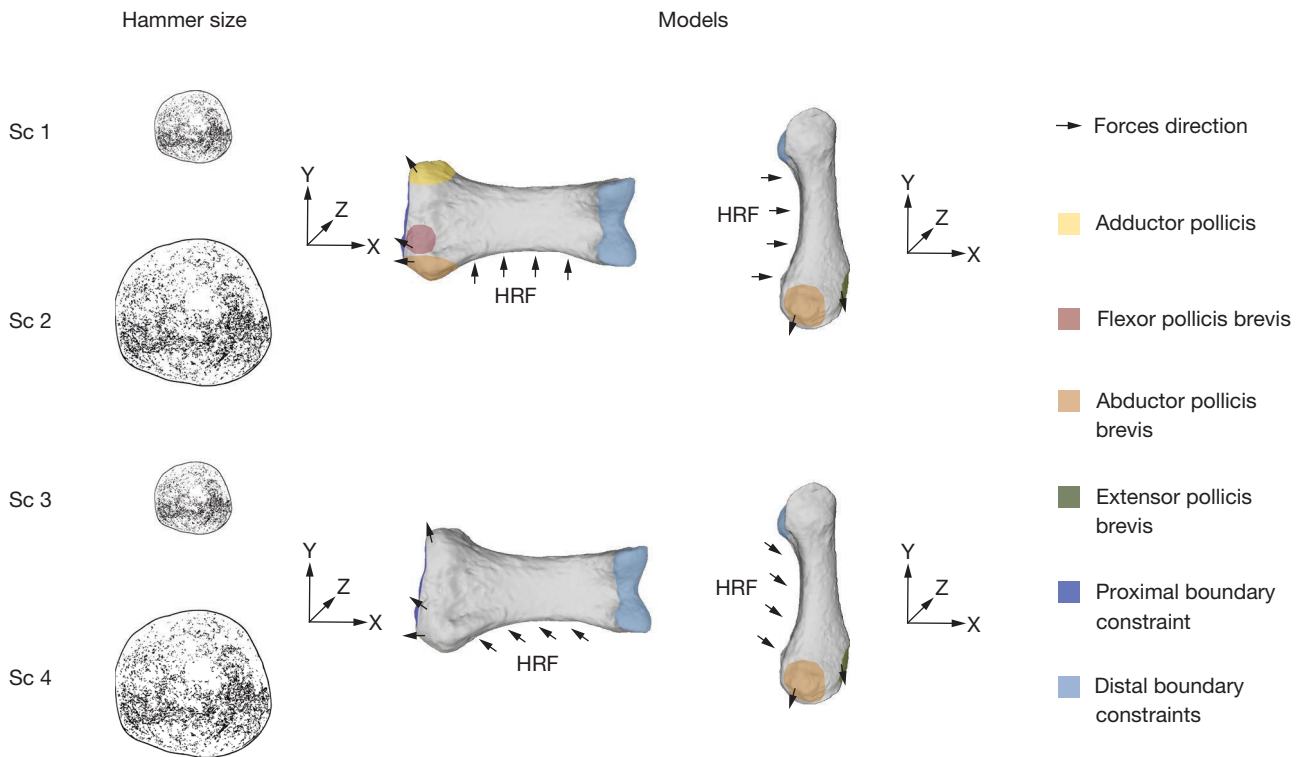


Fig. 2. — Free-body diagram of the phalanx in the different scenarios. This figure depicts the boundary conditions, areas of insertion of muscles, and direction of forces. For all loading configurations, joint reaction forces resulted from the rigid boundary constraints that were fixed at the distal joint in **X**, **Y** and **Z**-axes (light blue area), and at the proximal joint in the **X**-axis (dark blue area). The hammer reaction force (**HRF**) was applied to the entire palmar surface of the bone. 3.29 N for the **HRF** was simulated for **Sc 1** and **3**, and 7.65 N for **Sc 2** and **4**. Phalanges are shown in palmar (right) and radial (left) views.

Marzke *et al.* (1999) for the APB, FPB and AD muscles, and from Kikuchi (2010) for EPB. The PCSA for the chimpanzee was: FPB (1.40 cm²), ADP (2.50 cm²), EPB (1.44 cm²), and APB (1.80 cm²) (Marzke *et al.* 1999; Kikuchi 2010).

The PCSA for FPB, APB, and EPB muscles was then adjusted to the levels of muscle activity described in the electromyography (EMG) study of Marzke *et al.* (1998). These data correspond to the active (i.e., dominant) hand and were recorded at the strike, so all scenarios were simulated at that specific moment. Following Maier & Hepp-Reymond (1995), we assumed that the activity for the APB, not monitored in Marzke *et al.* (1998), was similar to EPB.

Muscle activity was considered during the use of two hammerstone sizes (400 g and 780 g, respectively, which are equivalent to 3.92 N and 7.65 N and represent the HRF). Although it would be interesting to include the loads from the core, they can significantly vary in size, as well as during the reduction sequence. More importantly, the reaction force corresponding to the core would need to be considerably higher than the hammerstone reaction force to alter the stress distribution on the PP1, which is the focus of the present study.

We simulated two tool orientations relative to the PP1: one with the long axis of the bone parallel to horizontal line (Sc 1 and 2), and the other at 45° (Sc 3 and 4), as shown in Figures 1 and 2.

The hands were modeled using a free-body diagram approach. A biomechanical model (Fig. 1b) was constructed based on data about hand posture, muscles active during hammerstone

use, the reaction forces from the hammerstone (HRF), and the joint reaction forces from metacarpal and distal phalanx (JRF_{mc} and JRF_d, respectively). Details of all loads involved are in Appendix 1.

Boundary conditions were defined to represent the fixed displacements that the models of PP1 experience during the loading scenarios. Once the models were solved, the joint reaction forces from the metacarpal (JRF_{mc}) and from the distal phalanx (JRF_d) were obtained. As boundary conditions have a great impact in the solution of the model, we intended to reproduce biological meaningful conditions for the PP1 to constrain the movements of the FEA models. The proximal part of the bone was fixed in the X dimension, and the distal part fixed in the X, Y and Z-axes (Fig. 2). All analyses were performed under these conditions (Appendix 1).

ANALYSIS OF VON MISES STRESS

We applied the recently-proposed quasi-ideal mesh (QIM) and its percentile values (M25, M50, M75, and M95) as a basis for our analysis (Marcé-Nogué *et al.* 2016). The use of a QIM mesh, corresponding to a mesh in which all the elements have practically the same size, facilitated between model comparisons, thus allowing the stress values obtained to be displayed as boxplots. Because the maximum value cannot be properly analyzed since it corresponds to artificially inflated values (Marcé-Nogué *et al.* 2015), here the M95 percentile is assumed as the peak value of stress following the concept introduced by Walmsley *et al.* (2013).

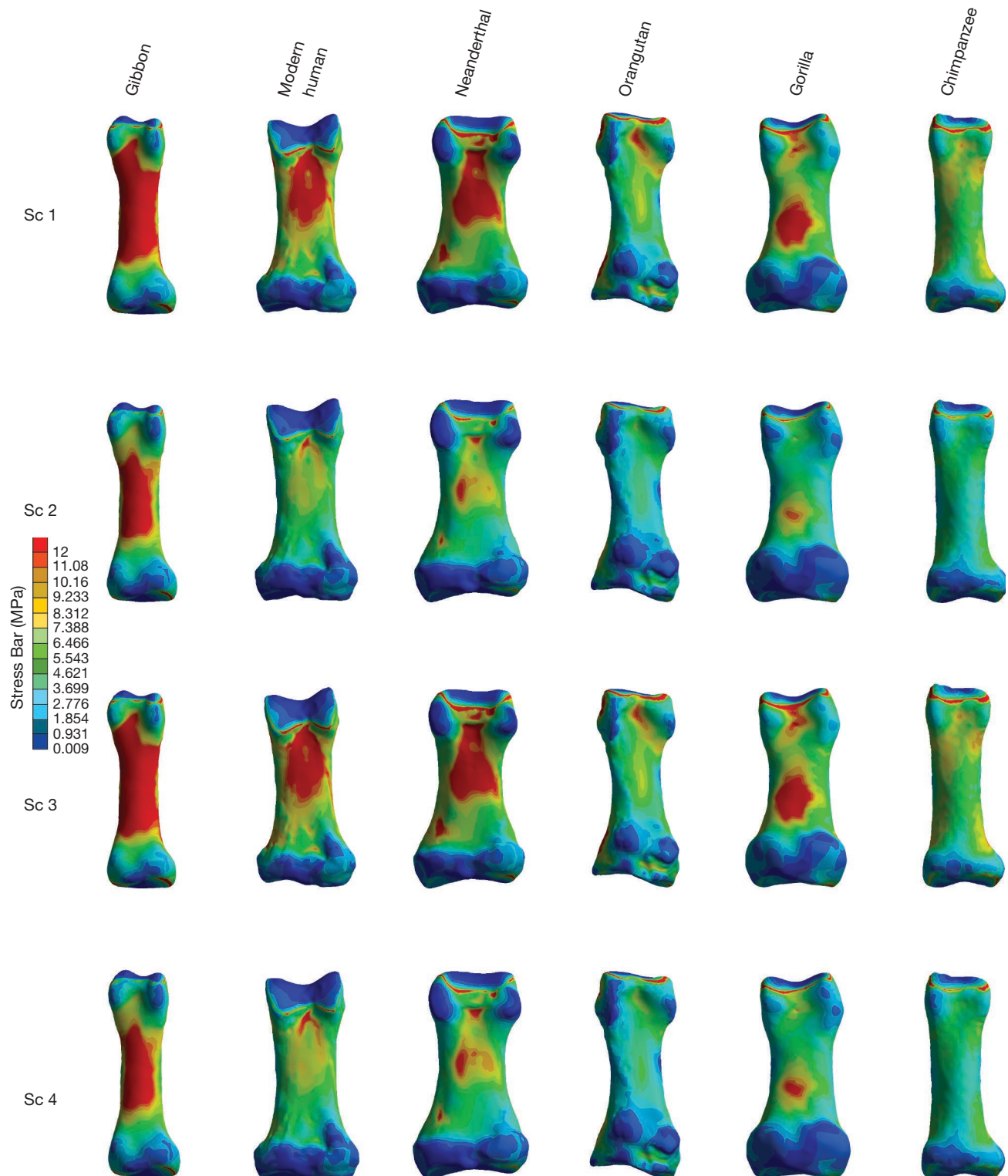


FIG. 3. — Von Mises stress maps for all analyzed species under different loading scenarios using the extant human as reference to scale the simulated muscular forces in all other specimens. Species are ordered from higher to lower peak stresses values. Phalanges are shown at the same length. MPa bar is set at 12 MPa.

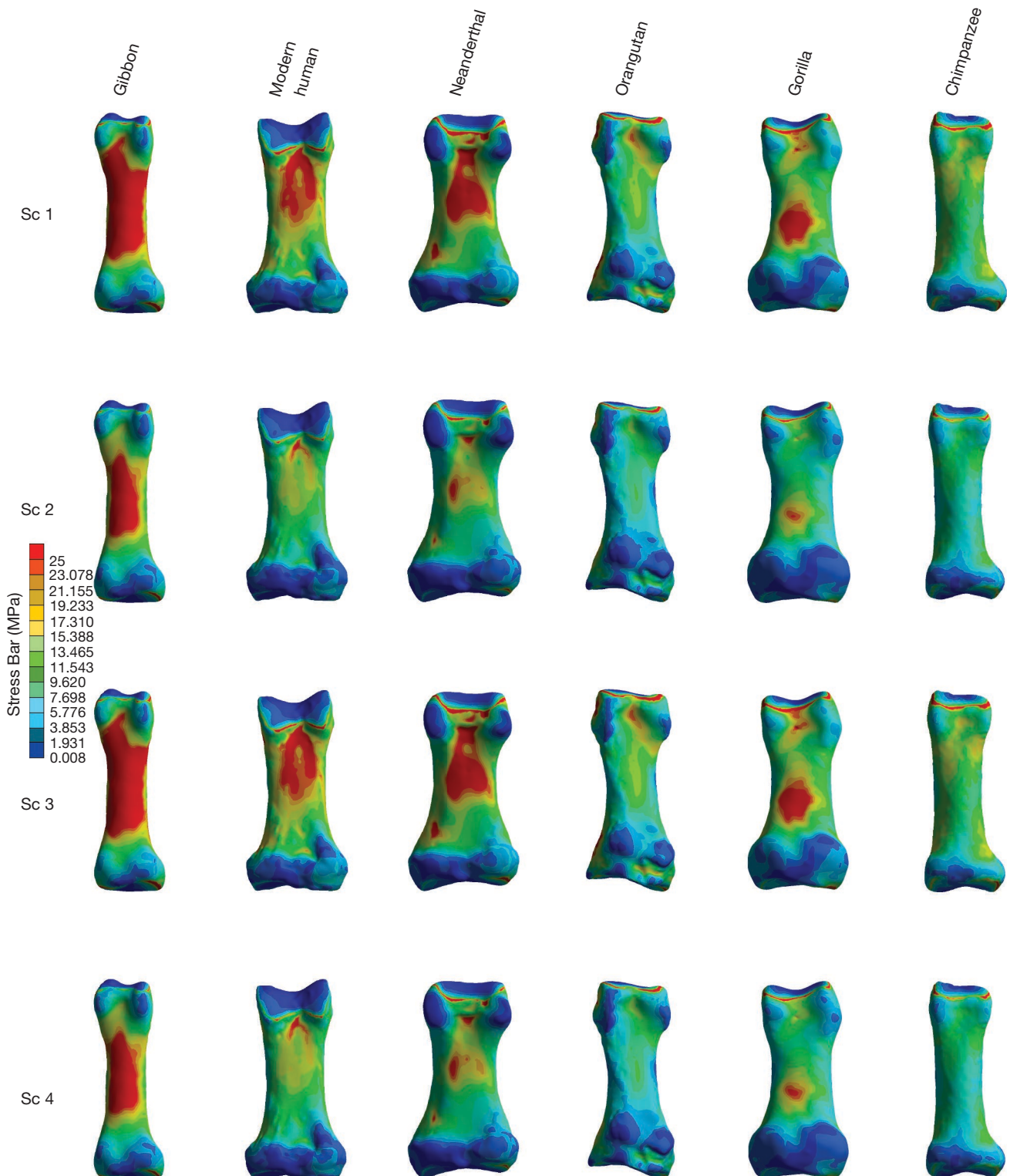


FIG. 4. — Von Mises stress maps for all analyzed species under different loading scenarios using the chimpanzee as reference to scale the simulated muscular forces in all other specimens. Species are ordered from higher to lower peak stresses values. Images are not scaled. MPa is set at 25 MPa.

In addition, a quantitative single measurement of the relative strength of the structure under study was used to summarize the strength of the whole phalanx as the mesh-weighted arithmetic mean (MWAM) and the mesh-weighted median (MWM). These last values are also required to estimate the percentage error of the arithmetic mean (PEofAM) and the percentage error of the median (PEofM), which are statistics used to ensure that our models were reliable QIMs as described in Marcé-Nogué *et al.* (2016). This information can be found in supplementary data Appendices 2 and 3.

RESULTS

The distribution of von Mises stress for each phalanx and scenario is shown in Figures 3 and 4. The specimen with the highest peak stress level was the gibbon, followed by the extant human, the Neanderthal, the orangutan, the gorilla and the chimpanzee representatives. This order was the same for all analyzed loading and scaling scenarios, except for the chimpanzee and gorilla, with the former having higher peak stresses than the gorilla in the first and second loading scenario (*Homo*-scaled), but lower in the remaining ones (Fig. 5).

Maximum von Mises stress values in the gibbon, extant human, Neanderthal and gorilla models were located in the center of the palmar surface of the phalanx body, decreasing towards the dorsal surface and the distal and proximal portions (Figs 3; 4). In these specimens, the lowest stress values were found in the joint areas and dorsal part, where the bone was not significantly affected by stress. Stress for the orangutan, chimpanzee and gorilla specimens were lower and more evenly distributed over the bone and, similarly to the humans and gibbon, did not affect the joint areas. In most cases, median stress values (MWM) for the extant human and Neanderthal representatives (Fig. 5) were lower and more focused than measured in chimpanzee, gorilla and orangutan (Figs 3; 4).

Peak and mean stress levels were considerably higher when the smaller hammerstone was simulated in all species (Fig. 5), while the effect of hammerstone orientation was less important. Overall, the effect of the hammerstone size was even greater than that related to the morphological differences between species (Fig. 5). Of all the scenarios, that showing the highest mean and peak values for all species was the one with the smaller hammerstone and the second bone orientation (Sc 3).

DISCUSSION

The objective of this study was to assess stress distribution in the pollical proximal phalanx (PP1) of the active hand during the simulated use of hammerstones in different Hominoidea species. In the analyses, we varied the size of the hammerstone, the orientation of the tool relative to the hand, and the muscular properties to see their effects in stress distribution over the bone. We expected human PP1 to behave more efficiently in every scenario, as we assumed its greater adaptation to tool-related behaviors. However, we found that, in all

cases, the human phalanx behaved as one among the most fragile bones, second only to the gibbon (Figs 3; 5). Stress distribution in the human PP1 was uneven and its concentration at the center of the shaft indicates that it is less resistant to loads during forceful precision grip and is more prone to structural failure. These results indicate that non-human hominids (i.e., gorilla, chimpanzee and orangutan) can better withstand loads exerted during this activity as compared to humans, although other key anatomical characteristics, for instance finger proportions, facilitate this activity in the later (Napier 1960; Rolian *et al.* 2011).

Our results suggest that stresses in the PP1 during tool-related behaviors were not the main driving force explaining the morphology of this bone, otherwise a different stress distribution would have very likely been observed in the human PP1. It is possible that the selective pressures acting on the thumb during stone tool production were not as consistently high to affect the morphology of this bone. Although other studies have found that the biomechanical stresses experienced by the thumb are high during this activity (Hamrick *et al.* 1998; Marzke *et al.* 1998; Key & Dunmore 2015; Williams-Hatala *et al.* 2018), there is a noticeably high variability between individuals in the observed kinematics (Rein *et al.* 2014), muscle activity (Marzke *et al.* 1998), and manual pressures (Williams *et al.* 2012; Williams-Hatala *et al.* 2018). These results raise the possibility that there were other stronger selective pressures acting on the PP1 that may not be related to stone-tool use. The argument that the evolution of the human hand was driven by selective pressures other than manipulative capabilities has been introduced in some previous studies (Alba *et al.* 2003; Almécija *et al.* 2010; Rolian *et al.* 2010; Heldstab *et al.* 2016). Specifically, the concept that the evolution of thumbs is linked to the evolution of toes (Rolian 2009; Rolian *et al.* 2010), thus to locomotor functions, which imply higher biomechanical demands than manipulation. Accordingly, locomotor functions would represent the primarily selective pressures shaping feet and hands in primates, including humans.

Even though the mean (MWM) and median (MWAM) stress values of humans were found relatively similar to those of non-human hominoids (i.e., gorilla, chimpanzee and orangutan) (Fig. 5), the poor stress distribution observed on the human representative resulted in a more fragile PP1. The variation in the distribution of stress among the specimens is probably related to differences in the morphology of the PP1 (Figs 3; 4). Future analyses deepen the relation between PP1 morphology and stress distribution under stone tool use conditions might shed some light into this link. Previous studies provide some guidance to this problem, as anatomical variations in hand morphology and structure within and among primates has been described, notably with respect to cortices thickness (Susman 1979; Tsegai *et al.* 2017), trabecular bone organisation (Lazenby *et al.* 2011; Chirchir *et al.* 2015; Matarazzo 2015; Skinner *et al.* 2015; Stephens *et al.* 2016), external dimensions and proportions (Napier 1962; Susman 1979; Key & Lycett 2018), and joint surface shape (Tocheri *et al.* 2003, 2005; Marchi *et al.* 2017).

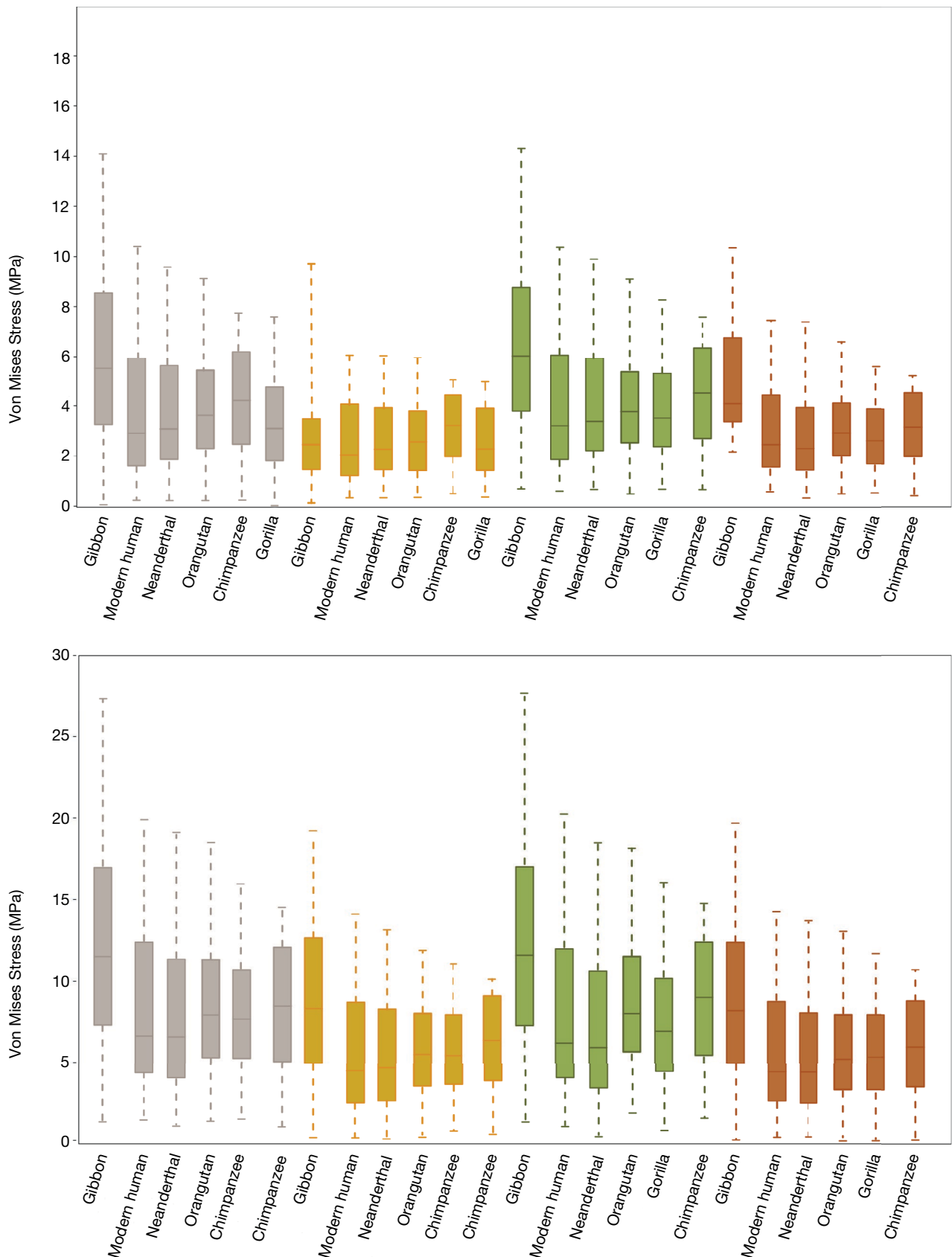


FIG. 5. — Box-plots of von Mises stress (MPa) distribution for all species under different scenarios, until Q95 (Sc 1 in grey, Sc 2 in yellow, Sc 3 in green and Sc 4 in red). The first row shows stress distribution of the models using the extant human as a reference to scale muscular forces in all other specimens, whereas the second one shows the results when the chimpanzee is used as a reference. Species are ordered from higher to lower peak stresses.

Does the force scaling of the non-human sample affect these results? While comprehensive knowledge is available about human muscles (e.g. Tuttle 1969; Marzke *et al.* 1998; Diogo *et al.* 2012b) and, to a lesser extent, in chimpanzees (Marzke *et al.* 1999; Kikuchi 2010), there are no analogous studies about the levels of muscular forces and activation patterns during the use of hammerstones for the other primate taxa considered here. To solve this problem, following Marcé-Nogué *et al.* (2013) and Fortuny *et al.* (2015), we scaled the muscular forces in the non-human hominins using the human and chimpanzee data as a reference, which allowed us to compare the behaviors of the PP1 from species that differ in size and morphology. In spite of this assumption, what makes the human (and gibbon) PP1 fragile is the stress distribution along the bone, which in this comparative analysis is not affected by the level of activation of the muscles. This becomes apparent when results from the two muscle scaling scenarios (human and chimpanzee) are compared: while stress values increase when using the chimpanzee muscles as reference, the stress distribution was very similar to the human scaling reference (Figs 3; 5).

A validation of FEA results against experimental data to see how precisely and accurately they reflect reality was not performed. Assumptions in our study for the non-human sample are related to muscle properties (tendon angles and forces), muscle activation patterns, and muscle function. Although detailed scenarios for each non-human representative would be ideal in such kind of analyses, these simplifications were necessary to evaluate the performance of each specimen which are difficult to access, such as muscle activation patterns during hammer use. Therefore, simulations were used to extract general patterns between species and should be interpreted in a comparative framework. This comparative approach has been successfully applied in several other studies using FEA (e.g. Serrano-Fochs *et al.* 2015; Püschel & Sellers 2016; Marcé-Nogué *et al.* 2017).

CONCLUSIONS

Non-human hominids (i.e., gorilla, chimpanzee and orangutan) can better withstand loads exerted during simulations of hard hammer percussion than humans. Among extant Hominoidea, the human PP1s were relatively fragile at the moment of strike. Our results suggest that in humans the forces exerted during forceful precision gripping did not act as a strong selective pressure affecting the morphology of the first pollical phalanx.

Acknowledgements

We want to thank the University of Barcelona's body donation service, especially Cristina Manzanares, Juan Antonio Camara, José Luis Ramón Cayuela, and Gemma Ramón Cayuela for their assistance. We are grateful to Dr. Tracy Kivell who gave us the micro-CT data of the orangutan phalanx and to the Senckenberg Museum in Frankfurt, where this

specimen is housed. We are also grateful to Clément Zanolli for the translation into French. We acknowledge NESPOS, and KUPRI for the CT scans of the non-human primates used in this study and the original providers of the material: Tennoji Zoo, Fukuoka City Zoo and the Fukuchiyama City Zoo. This work was supported by the General Directorate of Research of the Spanish Ministry of Science and Technology (MICINN-FEDER: grant number PGC2018-093925-B-C32); the Government of Catalonia (AGAUR: grant number 2017SGR 1040); the URV Project 2016 PFR-URV-B2-17; the Becas Chile Program of the Chilean National Commission for Scientific and Technological Research (CONICYT); the DFG, German Research Foundation (grant number KA 1525/9-2); and the Government of Catalonia's CERCA program. T.A.P was funded by the Leverhulme Trust Early Career Fellowship (grant number ECF-2018-264).

REFERENCES

- ALBA D. M., MOYÀ-SOLÀ S. & KÖHLER M. 2003. — Morphological affinities of the *Australopithecus afarensis* hand on the basis of manual proportions and relative thumb length. *Journal of Human Evolution* 44: 225-254. [https://doi.org/10.1016/S0047-2484\(02\)00207-5](https://doi.org/10.1016/S0047-2484(02)00207-5)
- ALMÉCJIA S., MOYÀ-SOLÀ S. & ALBA D. M. 2010. — Early Origin for Human-Like Precision Grasping: A Comparative study of Pollical distal Phalanges in Fossil Hominins. *Plos One* 5: 1-10. <https://doi.org/10.1371/journal.pone.0011727>
- BARDÒ A., CORNETTE R., BOREL A. & POUYDEBAT E. 2017. — Manual function and performance in humans, gorillas, and orangutans during the same tool use task. *American Journal of Physical Anthropology* 164: 1-16. <https://doi.org/10.1002/ajpa.23323>
- BUTZ K. D., MERRELL G. & NAUMAN E. A. 2012. — A Three-Dimensional Finite Element Analysis of Finger Joint Stresses in the MCP Joint While Performing Common Tasks. *HAND* 7: 341-345. <https://doi.org/10.1007/s11552-012-9430-4>
- CHIRCHIR H., KIVELL T. L., RUFF C. B., HUBLIN J. J., CARLSON K. J., ZIPFEL B. & RICHMOND B. G. 2015. — Recent origin of low trabecular bone density in modern humans. *Proceedings of the National Academy of Sciences* 112: 366-371. <https://doi.org/10.1073/pnas.1411696112>
- CIGNONI P., CALLIERI M., CORSINI M., DELLEPIANE M., GANOVELLI F. & RANZUGLIA G. 2008. — MeshLab: An open-source mesh processing tool. *Eurographics Italian chapter conference* vol. 2008, 129-136. <http://doi.org/10.2312/LocalChapterEvents/ItalChap/ItalianChapConf2008/129-136>
- DIOGO R., POTAU J. M., PASTOR J. F., DE PAZ F. J., FERRERO E. M., BELLO G., BARBOSA M. & WOOD B. A. 2011. — Photographic and descriptive musculoskeletal atlas of Gorilla: With notes on the attachments, variations, innervation, synonymy and weight of the muscles. Science Publishers, Enfield: 84.
- DIOGO R., POTAU J. M., PASTOR J. F., DE PAZ F. J., FERRERO E. M., BELLO G., BARBOSA M., AZIZ M. A., BURROWS A. M., ARIAS-MARTORELL J. & WOOD B. A. 2012a. — Photographic and descriptive musculoskeletal atlas of Gibbons and Siamese (Hylobates): With notes on the attachments, variations, innervation, synonymy and weight of the muscles. CRC Press, St. Helier: 168.
- DIOGO R., POTAU J. M., PASTOR J. F., DE PAZ F. J., FERRERO E. M., BELLO G., BARBOSA M., AZIZ M. A., BURROWS A. M., ARIAS-MARTORELL J. & WOOD B. A. 2013a. — Photographic and Descriptive Musculoskeletal Atlas of Chimpanzees: With notes on the attachments, variations, innervation, synonymy and weight of the muscles. CRC Press, Boca Raton: 157.

- DIOGO R., POTAU J. M., PASTOR J. F., DE PAZ F. J., FERRERO E. M., BELLO G., BARBOSA M., AZIZ M. A., ARIAS-MARTORELL J. & WOOD B. A. 2013b. — Photographic and Descriptive Musculoskeletal Atlas of Orangutans: With notes on the attachments, variations, innervation, synonymy and weight of the muscles. CRC Press, Boca Raton: 148.
- DIOGO R., RICHMOND B. G. & WOOD B., 2012b. — Evolution and homologies of primate and modern human hand and forearm muscles, with notes on thumb movements and tool use. *Journal of Human Evolution* 63: 64-78. <https://doi.org/10.1016/j.jhevol.2012.04.001>
- DOBLARÉ M., GARCIA J. M. & GÓMEZ M. J. J. 2004. — Modelling bone tissue fracture and healing: A review. *Engineering Fracture Mechanics* 71: 1809-1840. <https://doi.org/10.1016/j.engfrac-mech.2003.08.003>
- DUMONT E. R., GROSSE I. R. & SLATER G. J. 2009. — Requirements for comparing the performance of finite element models of biological structures. *Journal of Theoretical Biology* 256: 96-103. <https://doi.org/10.1016/j.jtbi.2008.08.017>
- FOLEY R. & LAHR M. M. 2003. — On stony ground: Lithic technology, human evolution, and the emergence of culture. *Evolutionary Anthropology* 12: 109-122. <https://doi.org/10.1002/evan.10108>
- FORTUNY J., MARCÉ-NOGUÉ J., HEISS E., SANCHEZ M., GIL L. & GALOBART À. 2015. — 3D Bite Modeling and Feeding Mechanics of the Largest Living Amphibian, the Chinese Giant Salamander *Andrias davidianus* (Amphibia: Urodela). *Plos One* 10: e0121885. <https://doi.org/10.1371/journal.pone.0121885>
- GOMMERY D. & SENUT B. 2006. — The terminal thumb phalanx of *Orrorin tugenensis* (Upper Miocene of Kenya). *Geobios* 39: 372-384. <https://doi.org/10.1016/j.geobios.2005.03.002>
- GREEN D. J. & GORDON A. D. 2008. — Metacarpal proportions in *Australopithecus africanus*. *Journal of Human Evolution* 54: 705-719. <https://doi.org/10.1016/j.jhevol.2007.10.007>
- GUMERT M. D. & MALAIJITNOND S. 2013. — Long-tailed macaques select mass of stone tools according to food type. *Philosophical Transactions of the Royal Society, B* 368: 20120413. <https://doi.org/10.1098/rstb.2012.0413>
- HAMRICK M. W., CHURCHILL S. E., SCHMITT D. & HYLANDER W. L. 1998. — EMG of the human flexor pollicis longus muscle: Implications for the evolution of hominid tool use. *Journal of Human Evolution* 34: 123-136. <https://doi.org/10.1006/jhev.1997.0177>
- HELDSTAB S. A., KOSONEN Z. K., KOSKI S. E., BURKART J. M., VAN SCHAIK C. P. & ISLER K. 2016. — Manipulation complexity in primates coevolved with brain size and terrestriality. *Scientific Reports* 6: 24528. <https://doi.org/10.1038/srep24528>
- HUNT K. D. 2004. — The special demands of great ape locomotion and posture, in Russon A. E. & Begun D. R. (eds), *The evolution of thought: Evolutionary origins of great ape intelligence*. Cambridge University Press, Cambridge: 172-189. <https://doi.org/10.1017/CBO9780511542299.013>
- JOUFFROY F. K., GODINOT M. & NAKANO Y. 1991. — Biometrical characteristics of primate hands in Preuschoft H. (ed.), *Hands of primates*. Springer-Verlag, Wien: 133-171. https://doi.org/10.1007/978-3-7091-6914-8_9
- KEY A. J. & DUNMORE C. J. 2015. — The evolution of the hominin thumb and the influence exerted by the non-dominant hand during stone tool production. *Journal of Human Evolution* 78: 60-69. <https://doi.org/10.1016/j.jhevol.2014.08.006>
- KEY A. J. & DUNMORE C. J. 2018. — Manual restrictions on Palaeolithic technological behaviours. *PeerJ* 6: e5399. <https://doi.org/10.7717/peerj.5399>
- KEY A. J. & LYCETT S. J. 2018. — Investigating interrelationships between Lower Palaeolithic stone tool effectiveness and tool user biometric variation: Implications for technological and evolutionary changes. *Archaeological and Anthropological Sciences* 10: 989-1006. <https://doi.org/10.1007/s12520-016-0433-x>
- KIKUCHI Y. 2010. — Comparative Analysis of Muscle Architecture in Primate Arm and Forearm. *Anatomia Histologia Embryologia* 39: 93-106. <https://doi.org/10.1111/j.1439-0264.2009.00986.x>
- KIVELL T. L., LEMELIN P., RICHMOND B. G. & SCHMITT D. (EDS) 2016. — *The evolution of the primate hand: Anatomical, developmental, functional and paleontological evidence*. Springer, New York: 483.
- LAUTENSCHLAGER S. 2016. — Reconstructing the past: Methods and techniques for the digital restoration of fossils. *Royal Society Open Science* 3: 160342. <https://doi.org/10.1098/rsos.160342>
- LAZENBY R. A., SKINNER M. M., HUBLIN J. J. & BOESCH C. 2011. — Metacarpal trabecular architecture variation in the chimpanzee (*Pan troglodytes*): Evidence for locomotion and tool-use? *Am. Journal of physical Anthropology* 144: 215-225. <https://doi.org/10.1002/ajpa.21390>
- MAIER M. A. & HEPP-REYMOND M. C. 1995. — EMG activation patterns during force production in precision grip - II. Muscular synergies in the spatial and temporal domain. *Experimental Brain Research* 103: 123-136. <https://doi.org/10.1007/BF00241970>
- MARCÉ-NOGUÉ J., DEMIGUEL D., FORTUNY J., DE ESTEBAN-TRIVIGNO S. & GIL L. 2013. — Quasi-homothetic transformation for comparing the mechanical performance of planar models in biological research. *Palaeontologia Electronica* 16: 1-15. <https://doi.org/10.26879/365>
- MARCÉ-NOGUÉ J., DE ESTEBAN-TRIVIGNO S., ESCRIG C. & GIL L. 2016. — Accounting for differences in element size and homogeneity when comparing Finite Element models: Armadillos as a case study. *Palaeontologia Electronica* 19: 1-22. <http://hdl.handle.net/2117/101929>
- MARCÉ-NOGUÉ J., FORTUNY J., GIL L. & SÁNCHEZ M. 2015. — Improving mesh generation in finite element analysis for functional morphology approaches. *Spanish Journal of Palaeontology* 30: 117-132. <https://doi.org/10.7203/sjp.30.1.17227>
- MARCÉ-NOGUÉ J., PÜSCHEL T. A. & KAISER T. M. 2017. — A biomechanical approach to understand the ecomorphological relationship between primate mandibles and diet. *Scientific Reports* 7: 8364. <https://doi.org/10.1038/s41598-017-08161-0>
- MARCHI D., PROCTOR D. J., HUSTON E., NICHOLAS C. L. & FISCHER F. 2017. — Morphological correlates of the first metacarpal proximal articular surface with manipulative capabilities in apes, humans and South African early hominins. *Comptes Rendus Palevol* 16 (5-6): 645-654. <https://doi.org/10.1016/j.crpv.2016.09.002>
- MARCY A. E., FRUCIANO C., PHILLIPS M. J., MARDON K. & WEISBECKER V. 2018. — Low resolution scans can provide a sufficiently accurate, cost-and time-effective alternative to high resolution scans for 3D shape analyses. *PeerJ* 6: e5032. <https://doi.org/10.7717/peerj.5032>
- MARZKE M. W. 2013. — Tool making, hand morphology and fossil hominins. *Philosophical Transactions of the Royal Society, B* 368: 20120414. <https://doi.org/10.1098/rstb.2012.0414>
- MARZKE M. W., MARZKE R. F., LINSCHEID R. L., SMUTZ P., STEINBERG B., REECE S. & AN K. N. 1999. — Chimpanzee thumb muscle cross sections, moment arms and potential torques, and comparisons with humans. *American Journal of Physical Anthropology* 110: 163-178.
- MARZKE M. W., TOTH N., SCHICK K. & REECE S. 1998. — EMG study of hand muscle recruitment during hard hammer percussion manufacture of Oldowan tools. *American Journal of Physical Anthropology* 105: 315-332.
- MATARAZZO S. 2013. — Manual pressure distribution patterns of knuckle-walking apes. *American Journal of Physical Anthropology* 152: 44-50. <https://doi.org/10.1002/ajpa.22325>
- MATARAZZO S. A. 2015. — Trabecular Architecture of the Manual Elements Reflects Locomotor Patterns in Primates. *Plos One* 10: e0120436. <https://doi.org/10.1371/journal.pone.0120436>
- MCCURRY M. R., EVANS A. R. & MCHENRY C. R. 2015. — The sensitivity of biological finite element models to the resolution of surface geometry: a case study of crocodilian crania. *PeerJ* 3: e988. <https://doi.org/10.7717/peerj.988>

- NAPIER J. R. 1960. — Studies of the hands of living primates. *Proceedings of the Zoological Society of London* 134: 647-657. <https://doi.org/10.1111/j.1469-7998.1960.tb05606.x>
- NAPIER J. R. 1962. — Fossil Hand Bones from Olduvai Gorge. *Nature* 196: 952-953. <https://doi.org/10.1038/196409a0>
- NIEWOEHNER W. A. 2001. — Behavioral inferences from the Skhul/Qafzeh early modern human hand remains. *Proceedings of the National Academy of Sciences* 98: 2979-2984. <https://doi.org/10.1073/pnas.041588898>
- PRUETZ J. D. & BERTOLANI P. 2007. — Savanna Chimpanzees, *Pan troglodytes verus*, Hunt with Tools. *Current Biology* 17: 412-417. <https://doi.org/10.1016/j.cub.2006.12.042>
- PÜSCHEL T. A. & SELLERS W. I. 2016. — Standing on the shoulders of apes: Analyzing the form and function of the hominoid scapula using geometric morphometrics and finite element analysis. *American Journal of Physical Anthropology* 159: 325-341. <https://doi.org/10.1002/ajpa.22882>
- RAYFIELD E. 2007. — Finite Element Analysis and Understanding the Biomechanics and Evolution of Living and Fossil Organisms. *Annual Review of Earth and Planetary Sciences* 35: 541-576. <https://doi.org/10.1146/annurev.earth.35.031306.140104>
- REIN R., NONAKA T. & BRIL B. 2014. — Movement Pattern Variability in Stone Knapping: Implications for the Development of Percussive Technologies. *Plos One* 9: e113567. <https://doi.org/10.1371/journal.pone.0113567>
- ROLIAN C. 2009. — Integration and evolvability in primate hands and feet. *Evolutionary Biology* 35: 36: 100-117. <https://doi.org/10.1007/s11692-009-9049-8>
- ROLIAN C., LIEBERMAN D. E. & HALLGRÍMSSON B. 2010. — The coevolution of human hands and feet. *Evolution* 64: 1558-1568. <https://doi.org/10.1111/j.1558-5646.2009.00944.x>
- ROLIAN C., LIEBERMAN D. E. & ZERMENO J. P. 2011. — Hand biomechanics during simulated stone tool use. *Journal of Human Evolution* 61: 26-41. <https://doi.org/10.1016/j.jhevol.2011.01.008>
- SACKS R. D. & ROY R. R. 1982. — Architecture of the hind limb muscles of cats: Functional significance. *Journal of Morphology* 173: 185-195. <https://doi.org/10.1002/jmor.1051730206>
- SAMUEL D. S., NAUWELAERTS S., STEVENS J. M. & KIVELL T. L. 2018. — Hand pressures during arboreal locomotion in captive bonobos (*Pan paniscus*). *Journal of Experimental Biology* 221: jeb170910. <https://doi.org/10.1242/jeb.170910>
- SERRANO-FOCHS S., DE ESTEBAN-TRIVIGNO S., MARCÉ-NOGUÉ J., FORTUNY J. & FARIÑA R. A. 2015. — Finite Element Analysis of the Cingulata Jaw: An Ecomorphological Approach to Armadillo's Diets. *Plos One* 10: e0120653. <https://doi.org/10.1371/journal.pone.0120653>
- SHREWSBURY M. M., MARZKE M. W., LINSCHEID R. L. & REECE S. P. 2003. — Comparative morphology of the pollical distal phalanx. *American Journal of Physical Anthropology* 121: 30-47. <https://doi.org/10.1002/ajpa.10192>
- SKINNER M. M., STEPHENS N. B., TSEGAI Z. J., FOOTE A. C., NGUYEN N. H., GROSS T., PAHR D. H., HUBLIN J.-J. & KIVELL T. L. 2015. — Human-like hand use in *Australopithecus africanus*. *Science* 347: 395-399. <https://doi.org/10.1126/science.1261735>
- SLIZIEWSKI A., FRIESS M. & SEMAL P. 2010. — Surface scanning of anthropological specimens: Nominal-actual comparison with low cost laser scanner and high end fringe light projection surface scanning systems. *Quartär* 57: 179-187.
- STEPHENS N. B., KIVELL T. L., GROSS T., PAHR D. H., LAZENBY R. A., HUBLIN J. J., HERSHKOVITZ I. & SKINNER M. M. 2016. — Trabecular architecture in the thumb of *Pan* and *Homo*: implications for investigating hand use, loading, and hand preference in the fossil record. *American Journal of Physical Anthropology* 161: 603-619. <https://doi.org/10.1002/ajpa.23061>
- SUSMAN R. L. 1979. — Comparative and functional morphology of hominoid fingers. *American Journal of Physical Anthropology* 50: 215-236. <https://doi.org/10.1002/ajpa.1330500211>
- SUSMAN R. L. 1988. — New postcranial remains from Swartkrans and their bearing on the functional morphology and behavior of *Paranthropus robustus* in Grine F. E. (ed.), *The evolutionary history of the "robust" australopithecines*. Aldine de Gruyter, New York: 149-172.
- SUSMAN R. L. & STERN J. T. 1979. — Telemetered electromyography of flexor digitorum profundus and flexor digitorum superficialis in *Pan troglodytes* and implications for interpretation of the O. H. 7 hand. *American Journal of Physical Anthropology* 50: 565-574. <https://doi.org/10.1002/ajpa.1330500408>
- TOCHERI M. W., MARZKE M. W., LIU D., BAE M., JONES G. P., WILLIAMS R. C. & RAZDAN A. 2003. — Functional capabilities of modern and fossil hominid hands: Three-dimensional analysis of trapezia. *American Journal of Physical Anthropology* 122: 101-112. <https://doi.org/10.1002/ajpa.10235>
- TOCHERI M. W., ORR C. M., JACOFSKY M. C. & MARZKE M. W. 2008. — The evolutionary history of the hominin hand since the last common ancestor of *Pan* and *Homo*. *Journal of Anatomy* 212: 544-562. <https://doi.org/10.1111/j.1469-7580.2008.00865.x>
- TOCHERI M. W., RAZDAN A., WILLIAMS R. C. & MARZKE M. W. 2005. — A 3D quantitative comparison of trapeziun and trapezoid relative articular and nonarticular surface areas in modern humans and great apes. *Journal of Human Evolution* 49: 570-586. <https://doi.org/10.1016/j.jhevol.2005.06.005>
- TSEGAI Z. J., STEPHENS N. B., TREECE G. M., SKINNER M. M., KIVELL T. L. & GEE A. H. 2017. — Cortical bone mapping: an application to hand and foot bones in hominoids. *Comptes Rendus Palevol* 16: 690-701. <https://doi.org/10.1016/j.crpv.2016.11.001>
- TUTTLE R. H. 1969. — Quantitative and functional studies on the hands of the Anthropoidea. *Journal of Morphology* 128: 309-363. <https://doi.org/10.1002/jmor.1051280304>
- VISALBERGHI E., SIRIANNI G., FRAGASZY D. & BOESCH C. 2015. — Percussive tool use by Taï Western chimpanzees and Fazenda Boa Vista bearded capuchin monkeys: A comparison. *Philosophical Transactions of the Royal Society, B* 370: 20140351. <https://doi.org/10.1098/rstb.2014.0351>
- WALMSLEY C. W., SMITS P. D., QUAYLE M. R., MCCURRY M. R., RICHARDS H. S., OLDFIELD C. C., WROE S., CLAUSEN P. D. & MCHENRY C. R. 2013. — Why the Long Face? The Mechanics of Mandibular Symphysis Proportions in Crocodiles. *Plos One* 8: e53873. <https://doi.org/10.1371/journal.pone.0053873>
- WILLIAMS E. M., GORDON A. D. & RICHMOND B. G. 2012. — Hand pressure distribution during Oldowan stone tool production. *Journal of Human Evolution* 62: 520-532. <https://doi.org/10.1016/j.jhevol.2012.02.005>
- WILLIAMS-HATALA E. M., HATALA K. G., GORDON M., KEY A., KASPER M. & KIVELL T. L. 2018. — The manual pressures of stone tool behaviors and their implications for the evolution of the human hand. *Journal of Human Evolution* 119: 14-26. <https://doi.org/10.1016/j.jhevol.2018.02.008>
- WUNDERLICH R. E. & JUNGERS W. L. 2009. — Manual digital pressures during knuckle-walking in chimpanzees (*Pan troglodytes*). *American Journal of Physical Anthropology* 139: 394-403. <https://doi.org/10.1002/ajpa.20994>
- WYNN T., HERNANDEZ-AGUILAR R. A., MARCHANT L. F. & McGREW W. C. 2011. — “An ape’s view of the Oldowan” revisited. *Evolutionary Anthropology* 20: 181-197. <https://doi.org/10.1002/evan.20323>
- WYNN T. & McGREW W. C. 1989. — An ape’s view of the Oldowan. *Man* 24: 383-398. <https://doi.org/10.2307/2802697>
- YOUNG R. W. 2003. — Evolution of the human hand: The role of throwing and clubbing. *Journal of Anatomy* 202: 165-174. <https://doi.org/10.1046/j.1469-7580.2003.00144.x>

Submitted on 17 August 2019;
accepted on 18 October 2019;
published on 10 August 2020.

APPENDIX 1. – Loads applied to the models for each one of the species under analysis and simulated loading scenarios. Abbreviations: **a**, forces (**N**) and angles (Θ) relative to the longitudinal axes of the bone; **b**, muscle forces for the human and chimpanzee reference models, respectively, are separate by a slash; **c**, force reactions in the proximal and distal joints were scaled to remove size effects when computing stress distributions.

Specimen	SC	HRFa	FPB HS /FPB PT ^b	AP HS /AP PT ^b	EPB HS /EPB PT ^b	ABP HS /ABP PT ^b	JRFd ^c	JRFmc ^c
		N	θ	N	θ	N	θ	N
Modern Human	1	3.92	90	17.95/37.20	45	38.79/66.43	61.2	4.33/28.75
	2	7.65	90	13.49/27.95	45	29.15/49.91	61.2	2.74/18.18
	3	3.92	45	17.95/37.20	45	38.79/66.43	61.2	4.33/28.75
	4	7.65	45	13.49/27.95	45	29.15/49.91	61.2	2.74/18.18
Neanderthal	1	3.92	90	14.47/29.99	45	31.28/53.56	61.2	3.49/23.18
	2	7.65	90	10.87/22.54	45	23.50/40.24	61.2	2.21/14.66
	3	3.92	45	14.47/29.99	45	31.28/53.56	61.2	3.49/23.18
	4	7.65	45	10.87/22.54	45	23.50/40.24	61.2	2.21/14.66
Chimpanzee	1	3.92	90	18.34/38.01	45	39.64/67.88	61.2	–
	2	7.65	90	13.78/28.56	45	29.78/51.00	61.2	–
	3	3.92	45	18.34/38.01	45	39.64/67.88	61.2	–
	4	7.65	45	13.78/28.56	45	29.78/51.00	61.2	–
Gorilla	1	3.92	90	24.78/51.36	45	53.55/91.71	61.2	5.97/39.69
	2	7.65	90	18.62/38.59	45	40.24/68.91	61.2	3.78/25.10
	3	3.92	45	24.78/51.36	45	53.55/91.71	61.2	5.97/39.69
	4	7.65	45	18.62/38.36	45	40.24/68.91	61.2	3.78/25.10
Orangutan	1	3.92	90	19.74/40.91	45	42.66/73.06	61.2	–
	2	7.65	90	14.83/30.74	45	32.06/54.90	61.2	–
	3	3.92	45	19.74/40.91	45	42.66/73.06	61.2	–
	4	7.65	45	14.83/30.74	45	32.06/54.90	61.2	–
Gibbon	1	3.92	90	7.08/14.66	45	15.29/26.1	61.2	–
	2	7.65	90	5.32/11.02	45	11.49/19.68	61.2	–
	3	3.92	45	7.08/14.66	45	15.29/26.19	61.2	–
	4	7.65	45	5.32/11.02	45	11.49/19.68	61.2	–

APPENDIX 2. — Number of elements (N elements), mesh-weighted arithmetic mean (**MWAM**), mesh-weighted median (**MWM**), quartiles values (**Q25**, **50**, **75** and **95**), percentage error of the arithmetic mean (**PEofAM**) and percentage error of the median (**PEofM**) for each species and loading scenario, under human-scaled conditions.

INDIVIDUAL	SCENARIO	N of Elements	MWAM	MWM	Q25	Q50	Q75	M95	PEofAM	PEofM
Modern Human	1	225689	3.7540	2.6128	1.3997	2.6690	5.6844	10.0261	0.7130	2.1509
Modern Human	2	225729	2.5238	1.7800	0.9680	1.8227	3.8100	6.6442	0.7309	2.3997
Modern Human	3	225689	3.8349	2.6530	1.4269	2.7080	5.8135	10.2790	0.7100	2.0714
Modern Human	4	225710	2.6876	1.8662	1.0241	1.9051	4.0670	7.1455	0.7225	2.0867
Neanderthal	1	240478	3.7401	2.7851	1.5604	2.8336	5.3814	9.6489	1.6161	1.7432
Neanderthal	2	240469	2.5277	1.8985	1.0995	1.9326	3.6118	6.4210	1.5858	1.7975
Neanderthal	3	240469	3.8275	2.8449	1.6271	2.8931	5.4883	9.8692	1.6163	1.6943
Neanderthal	4	240471	2.6708	1.9879	1.1443	2.0203	3.8108	6.8892	1.6184	1.6299
Chimpanzee	1	160103	4.1812	3.9750	2.2535	4.0610	5.9939	7.6454	0.0015	2.1631
Chimpanzee	2	160104	2.8698	2.7413	1.5694	2.8039	4.0960	5.1944	0.0004	2.2836
Chimpanzee	3	160046	4.2475	4.0192	2.2864	4.1141	6.0832	7.7941	0.0148	2.3599
Chimpanzee	4	160104	3.0042	2.8468	1.6410	2.9113	4.2753	5.4869	0.0164	2.2646
Gorilla	1	225710	2.6876	1.8662	1.0241	1.9051	4.0670	7.1455	0.7225	2.0867
Gorilla	2	327267	2.4440	2.1049	1.3316	2.1522	3.1882	5.1728	0.1482	2.2471
Gorilla	3	327267	3.7738	3.1737	1.9572	3.2548	5.0131	8.1784	0.1610	2.5570
Gorilla	4	327267	2.6870	2.2688	1.3987	2.3215	3.5807	5.7799	0.1603	2.3228
Orangutan	1	199857	4.0409	3.3878	2.1630	3.4804	5.2597	9.1689	0.6450	2.7344
Orangutan	2	199857	2.7519	2.3201	1.5089	2.3899	3.5526	6.1413	0.6300	3.0085
Orangutan	3	199813	4.1216	3.4543	2.2075	3.5543	5.3691	9.3611	0.6596	2.8941
Orangutan	4	199813	2.9129	2.4571	1.5893	2.5330	3.7670	6.5330	0.6369	3.0885
Gibbon	1	311431	6.3313	5.4576	3.2272	5.5294	8.5269	14.0750	0.1785	1.3156
Gibbon	2	311442	4.3431	3.7514	2.2259	3.8016	5.8425	9.6143	0.1738	1.3370
Gibbon	3	311442	6.4105	5.5281	3.2583	5.6069	8.6284	14.2694	0.1767	1.4247
Gibbon	4	311442	4.5087	3.9023	2.3007	3.9605	6.0438	10.0180	0.1783	1.4927

APPENDIX 3. — Mesh-weighted arithmetic mean (**MWAM**), mesh-weighted median (**MWM**), quartiles values (**Q25**, **50**, **75** and **95**), percentage error of the arithmetic mean (**PEofAM**) and percentage error of the median (**PEofM**) for each species and loading scenario, under chimpanzee-scaled conditions.

SPECIE	SCENARIO	N of Elements	MWAM	MWM	Q25	Q50	Q75	M95	PEofAM	PEofM
Chimpanzee	1	160104	8.0122	7.6599	4.2909	7.8345	11.4830	14.6530	0.0387	2.2794
Chimpanzee	2	160104	5.7312	5.4881	3.0880	5.6170	8.2101	10.4363	0.0341	2.3483
Chimpanzee	3	160104	8.0771	7.7090	4.3233	7.8865	11.5780	14.7960	0.0417	2.3024
Chimpanzee	4	160104	5.8607	5.5899	3.1557	5.7215	8.3844	10.7170	0.0419	2.3534
Modern Human	1	225743	7.5983	5.4469	3.0316	5.5620	11.3770	19.8150	0.7364	2.1135
Modern Human	2	225743	5.3623	3.8494	2.1389	3.9323	8.0325	13.9420	0.7334	2.1536
Modern Human	3	225720	7.6821	5.4907	3.0617	5.6072	11.4980	20.0690	0.7328	2.1222
Modern Human	4	225689	5.5209	3.9340	2.1951	4.0167	8.2813	14.4290	0.7156	2.1020
Neanderthal	1	240469	7.5408	5.7398	3.1415	5.8463	10.7260	19.1300	1.6003	1.8559
Neanderthal	2	240461	5.3229	4.0535	2.2448	4.1316	7.5691	13.4480	1.5817	1.9264
Neanderthal	3	240469	7.6103	5.7887	3.1663	5.8917	10.8170	19.3540	1.6076	1.7799
Neanderthal	4	240460	5.4615	4.1433	2.2936	4.2210	7.7516	13.9010	1.6017	1.8739
Gorilla	1	327267	7.5848	6.5180	4.1315	6.6614	10.0078	15.9652	0.1499	2.2001
Gorilla	2	327267	5.3112	4.5847	2.9071	4.6850	6.9811	11.1340	0.1473	2.1877
Gorilla	3	327267	7.7032	6.5956	4.1665	6.7425	10.1980	16.2770	0.1521	2.2272
Gorilla	4	327267	5.5459	4.7386	2.9746	4.8493	7.3571	11.7390	0.1536	2.3361
Orangutan	1	199857	7.9291	6.5783	4.2297	6.7471	10.3643	18.0617	0.6350	2.5660
Orangutan	2	199857	5.6296	4.6925	3.0326	4.8168	7.3231	12.7377	0.6308	2.6495
Orangutan	3	199782	8.0098	6.6472	4.2716	6.8239	10.4630	18.2554	0.6575	2.6582
Orangutan	4	199782	5.7884	4.8286	3.1119	4.9592	7.5206	13.1060	0.6481	2.7040
Gibbon	1	311442	12.1044	10.4260	6.1984	10.5940	16.2630	26.8950	0.1734	1.6114
Gibbon	2	311431	8.6667	7.4740	4.4483	7.5885	11.6390	19.2340	0.1762	1.5325
Gibbon	3	311442	12.1825	10.4940	6.2322	10.6650	16.3650	27.0820	0.1744	1.6295
Gibbon	4	311442	8.8241	7.6109	4.5179	7.7380	11.8330	19.6238	0.1753	1.6704